Na and Ca Channels in a Transformed Line of Anterior Pituitary Cells

D. R. MATTESON and C. M. ARMSTRONG

From the Department of Physiology, University of Pennsylvania, Philadelphia, Pennsylvania 19104 and The Marine Biological Laboratory, Woods Hole, Massachusetts 02543

ABSTRACT The ionic conductances of GH3 cells, a transformed line from rat anterior pituitary, have been studied using the whole-cell variant of the patch-clamp technique (Hamill et al., 1981). Pipettes of very low resistance were used, which improved time resolution and made it possible to control the ion content of the cell interior, which equilibrated very rapidly with the pipette contents. Time resolution was further improved by using series resistance compensation and "ballistic charging" of the cell capacitance. We have identified and partially characterized at least three conductances, one carrying only outward current, and the other two normally inward. The outward current is absent when the pipette is filled with Cs^+ instead of K^+, and has the characteristics of a voltage-dependent potassium conductance. One of the two inward conductances (studied with Cs^+ inside) has fast activation, inactivation and deactivation kinetics, is blocked by tetrodotoxin (TTX), and has a reversal potential at the sodium equilibrium potential. The other inward current activates more slowly and deactivates with a quick phase and a very slow phase after a short pulse. Either Ca^{++} or Ba^{++} serves as current carrier. During a prolonged pulse, current inactivates fairly completely if there is at least 5 mM Ca^{++} outside, and the amplitude of the current tails following the pulse diminishes with the time course of inactivation. When Ba^{++} entirely replaces Ca^{++} in the external medium, there is no inactivation, but deactivation kinetics of Ca channels vary as pulse duration increases: the slow phase disappears, the fast phase grows in amplitude. Inactivation (Ca^{++} outside) is unaltered by 50 mM EGTA in the pipette: inactivation cannot be the result of internal accumulation of Ca^{++}.

INTRODUCTION

A wide variety of cells are known to exhibit electrical activity. In recent years it has become apparent that many types of endocrine cells, including cells of the anterior pituitary, generate signals resembling nerve action potentials. Action potentials have been recorded from GH3 cells (Kidokoro, 1975; Biales et al., 1977), which are a transformed line of anterior pituitary cells, and from dispersed cells of the adult gland (Taraskevich and Douglas, 1977). The spikes of GH3 cells have a prominent Ca component which is tetrodotoxin (TTX) resistant and

Address reprint requests to Dr. C. M. Armstrong, Dept. of Physiology, University of Pennsylvania, Philadelphia, PA 19104.

J. GEN. PHYSIOL. © The Rockefeller University Press · 0022-1295/84/03/0371/24 $1.00

Volume 83 March 1984 371–394

could, in some cases, be blocked by the Ca channel blockers D600 or Mn^{++} (Kidokoro, 1975; Taraskevich and Douglas, 1980). Thyrotrophin-releasing factor and other secretagogues increase spike frequency (Taraskevich and Douglas, 1980), and it may be that action potentials function primarily to regulate the influx of calcium ions required for secretion. In preparation for studying the mechanism by which secretagogues alter membrane conductances, we have identified and characterized the channels responsible for electrical activity in GH3 cells.

The whole-cell variant of the patch-clamp technique (Hamill et al., 1981) is a powerful new tool which makes it possible to accurately record membrane currents under voltage clamp from very small cells. We have used this method in GH3 cells to describe at least one outward current carried through K channels, and two components of inward current carried through Na and Ca channels (see also Hagiwara and Ohmori, 1982; Dubinsky and Oxford, 1982; Dufy and Barker, 1982). As pointed out by Hagiwara and Ohmori (1982), GH3 cells are particularly valuable for studying Ca currents, which can be accurately recorded without contamination from other currents. This has made it possible for us to demonstrate that the Ca channel inactivates, and to describe aspects of the inactivation mechanism. Inactivation of Ca channels in GH3 cells does not seem to result from Ca accumulation inside the cell, as proposed in paramecium (Brehm and Ekert, 1978) and *Aplysia* (Tillotson, 1979), although inactivation does require the presence of external Ca^{++}. A preliminary account of these results has appeared elsewhere (Matteson and Armstrong, 1983).

METHODS

Cell Culture

Patch-clamp experiments were performed on GH3 cells obtained from the American Type Culture Collection (No. CCL 82.1) at passage No. 20. The cells were grown in 35-mm plastic petri dishes with 10 parts Dulbecco's modified Eagle's medium and one part NCTC 135 (Gibco Laboratories, Grand Island, NY), supplemented with 5% fetal bovine serum and 1% glutamine. The medium was usually replaced every other day and the cells were subcultivated and split about once a week. The growth vessels were maintained in a humidified atmosphere of 92% air and 8% CO_2 at 37°C.

Solutions

The medium in the selected culture dish was changed to a protein-free recording solution at the beginning of the experiment. The compositions of the recording solutions are shown in Table I. Most solutions contained an elevated calcium concentration to facilitate the formation of gigaseals. In the text, solutions are specified as external//internal. We will refer to the pipette-filling solution as the internal solution since Fenwick et al. (1982*a*) have shown that there is rapid equilibration between the pipette solution and the cell cytoplasm, a conclusion with which we agree (see below). Solutions were buffered to pH 7.3 and passed through 0.2-μm Millipore filters before use. Experiments were performed at room temperature (22–26°C).

Electrodes

Patch electrodes were fabricated with a double pull on a David Kopf vertical electrode puller, followed by light firepolishing on a homemade microforge (Hamill et al., 1981).

The tip size of the electrode before and after firepolishing was calibrated by determining the pressure required to blow air bubbles out of the electrode tip into acetone. By carefully controlling the voltage applied across the heating filament during the second pull and the heat applied during polishing, we consistently obtained electrodes with the desired resistance. Bubble thresholds before polishing were typically 1.25–1.35 atm, and 1.5–1.7 atm after polishing.

Particularly for whole-cell current recordings, it is important to minimize the electrode resistance, which is in series with the membrane capacitance. The product of this resistance and the membrane capacitance determines the time required to impose a voltage-clamp step. We have, in fact, found that this series resistance is often much higher than the resistance of the electrode in free solution, presumably because the electrode tip is partially occluded by cellular material. Empirically, the series resistance is lower with borosilicate

TABLE I

Recording Solutions

External solutions	Na*	K	Ca	Ba	Mg	Tris	Hepes
130 Na, 10 Ca	130‡	5	10	—	2	—	10
130 Na, 10 Ba	130	5	—	10	2	—	10
140 Na, 2 Ca, 3 Mg	140	—	2	—	3	—	10
140 Na, 5 Mg	140	—	—	—	5	—	10
140 Na, 2 Ca	140	—	2	—	—	—	10
140 Na, 5 Ca	140	—	5	—	—	—	10
35 Ca	—	5	35	—	2	104	—
35 Ba	—	5	—	35	2	104	—
35 Ba, 5 Ca	—	5	5	35	2	94	—

Internal solutions	Na	K	Cs	Mg	EGTA	Hepes
140 K	—	140	—	2	11	10
130 K, 10 Cs	—	130	10	2	1.5	10
140 Cs, 11 EGTA	—	—	140	2	11	10
130 Cs, 20 EGTA	—	—	130	2	20	5
110 Cs, 20 Na, 20 EGTA	20	—	110	2	20	10
150 Cs	—	—	150	2	—	5
80 Cs, 50 EGTA	—	—	80	2	50	5
140 Na	140	—	—	2	10	10

* Chloride salts of all cationic species were used.

‡ Concentrations are in millimolar. The osmolality of all solutions was adjusted to 300 mosmol.

electrodes than with those made from soda-lime glass. The experiments described here were all performed with low-resistance borosilicate electrodes, 0.8–1.5 MΩ after polishing.

Electronics

The patch-clamp amplifier for these experiments was made by us and incorporates most of the features of the standard design (Hamill et al., 1981). We used a Burr-Brown Research Corp. (Tucson, AZ) 3523 op-amp as the current-to-voltage converter, although a 356 seemed to perform just as well in our application. The command voltage for voltage-clamp purposes was applied to the noninverting input of the *I-V* converter. To record macroscopic currents, gain was sacrificed for frequency response by using a relatively low feedback resistance (20–100 MΩ). The current signal was conditioned by a single-pole low-pass filter with a cutoff frequency of 5 kHz.

Two techniques were used to enhance the speed with which a voltage step would be applied to the cell membrane. The first technique involved feeding current to the *I-V* converter through a very small capacitor. The other side of the capacitor was driven by a shaped voltage step that was derived from the command voltage. The net effect is that the membrane capacitance is ballistically charged. If the step is of exactly the right shape, a voltage change is imposed on the membrane with no intervention from the *I-V* converter: all of the charging current is supplied through the small capacitor on the input. Our patch clamp also incorporated circuitry for series resistance compensation. The series resistance was sometimes calculated, as described below, but compensation was usually applied empirically, by speeding up the capacity transient as much as possible without producing an overshoot. This usually required compensation for 5–10 MΩ which, as the calculations below suggest, was somewhat more than the actual series resistance, giving an error of as much as 5 mV for large currents. Capacity transients had time constants of 50–100 μs before compensation and 35–50 μs after.

Calculation of Series Resistance

The resistance in series with the membrane capacitance was estimated as follows. First, the capacitive current generated by a hyperpolarizing voltage-clamp step recorded before breaking into the cell was subtracted from that recorded after. The result is a measure of the current across the membrane capacitance (I_C). I_C was then integrated to estimate the amount of charge required to hyperpolarize the membrane, and this value was used to calculate cell capacitance ($C = Q/V$). Finally, the series resistance was calculated as the time constant of I_C divided by the capacitance. In one typical case, a 1.3-MΩ electrode resulted in a series resistance of 3 MΩ in the whole-cell recording configuration.

Data Acquisition

An LSI-11/23 computer (Digital Equipment Corp., Maynard, MA) was used to acquire, store, and analyze the data. In collaboration with R. J. Bookman, we designed and built the hardware necessary to interface the analog electronics with the computer. Briefly, the interface performs the following four major functions: (*a*) data sampling through a 12- or 14-bit analog-to-digital converter at rates that can exceed 250 kHz, (*b*) pulse generation, utilizing onboard RAM to allow up to 512 voltage changes of arbitrary duration, (*c*) display, providing two vertical channels and a time base, and (*d*) timing, with a real time clock.

Currents were either stored unaltered or the linear components of capacitive and ionic current were subtracted out with a P/2 procedure (cf. Armstrong and Bezanilla, 1974).

Experimental Procedure

To balance out junction potentials, the patch electrode was placed in the chamber and the DC command potential was adjusted until the recorded current was zero. This zero-current point was taken as the baseline for setting cell voltage with the clamp circuit. To record macroscopic currents, a gigaseal was first obtained by applying gentle suction to the interior of the patch electrode. The DC potential in the pipette was then set to the desired holding potential (−70 or −80 mV) and further suction was applied to rupture the patch of membrane under the electrode tip. Breaking into the cell was evidenced by an increase in the magnitude and time course of the capacitive current generated by small hyperpolarizing voltage-clamp steps. Under these conditions, the *I-V* converter measures currents flowing through the entire cell surface.

RESULTS

Major Current Components

At least three major components of membrane current can be recognized after step depolarization of a voltage-clamped GH3 cell, as illustrated in Fig. 1. The cell was bathed in 130 Na, 10 Ca, with 130 K, 10 Cs internally (130 Na, 10 Ca// 130 K, 10 Cs). Between the arrows, membrane voltage (V_m) was changed to +20 mV from a holding potential of −70 mV. At +20 mV there is (*a*) a rapidly activating inward current which is followed by (*b*) a sustained outward current. Repolarization to −70 mV causes (*c*) a large, slowly decaying tail of inward current. We will show below that the fast, transient inward current (component *a*) is absent when Na ions are removed and is blocked by TTX, which indicates that Na channels carry this current.

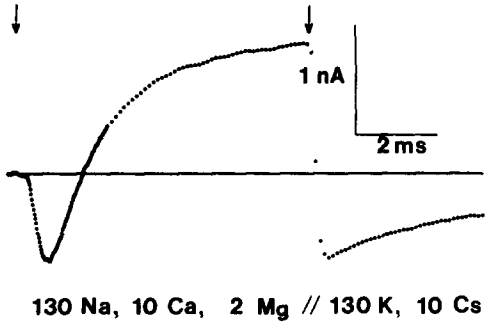

FIGURE 1. Major current components in GH3 cells. Membrane voltage was stepped to +20 mV between the arrows, from a holding potential of −70 mV. During the step there is a rapidly activating inward current, followed by a sustained outward current. After repolarization there is a large slowly decaying tail of inward current. Solutions were 130 Na, 10 Ca//130 K, 10 Cs (outside//inside). Preparation FE073R.

The outward current (component *b*) is very large with 140 K internally, and was reduced in Fig. 1 by including 10 mM Cs^+ in the internal solution. Outward current was practically absent when all K^+ was replaced by Cs^+, and it was blocked in a time-dependent manner by internal Ba^{++}, which suggests that K channels carry this current (cf. Adelman and Senft, 1966; Bezanilla and Armstrong, 1972; Armstrong and Taylor, 1980; Eaton and Brodwick, 1980). We have not specifically identified the type (or types) of K channels present in these cells, but they are clearly voltage dependent, with characteristics similar to K channels in nerve.

The amplitude of the slow inward tail (component *c*) depends on the external Ca^{++} concentration, as shown below, and is larger when Ca^{++} is replaced by Ba^{++}, which indicates that Ca channels are the basis for this current.

Two Components of Inward Current

The remainder of the experiments reported here are concerned with the inward

currents in GH3 cells (components *a* and *c* in Fig. 1), and we eliminated the outward current by substituting Cs^+ for K^+ in all pipette solutions. To avoid confusion, we will refer to "pulse currents" and "tail currents," meaning, respectively, the currents during a step depolarization and after return to the holding potential. Both pulse and tail currents are usually inward in the presence of internal Cs^+.

The behavior of the inward currents during steps to the indicated voltages is illustrated in Fig. 2, for a cell in 130 Na, 10 Ca//140 Cs, 11 EGTA. At +10 mV or more, the pulse current increases rapidly to a peak ~1 ms after the step. It then decays rapidly for ~1 ms, and slowly thereafter, leaving a substantial inward

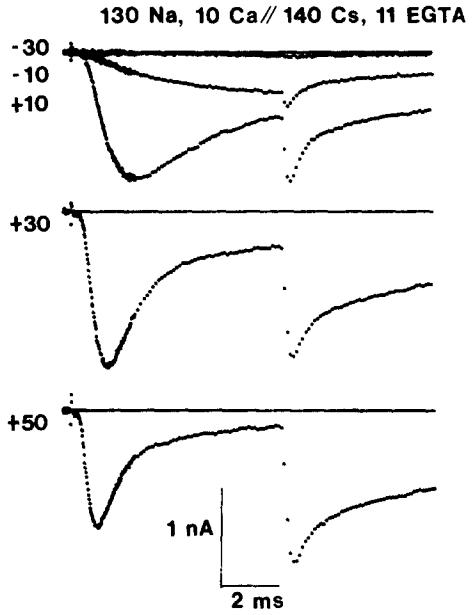

FIGURE 2. Inward current in GH3 cells, during steps to the indicated voltages. All traces show inward current during the pulse and a large current tail afterwards. The initial amplitude of the tail increases with voltage up to +30 mV. 130 Na, 10 Ca//140 Cs, 11 EGTA. Holding potential: −70 mV. Preparation JA203R.

current at pulse end. After repolarization to −70 mV, the tail current in this experiment has both a fast and a slow phase of decay (cf. Fig. 1, in which the fast phase is absent). The initial amplitude of the tail increases with the amplitude of the activating step up to +30 mV.

The inward currents in Fig. 2 result from the activity of two types of voltage-dependent channels, one of which is TTX sensitive. Fig. 3*A* shows current during a depolarization to +20 mV under conditions identical to those of Fig. 2. When TTX is present in the bathing solution (≥50 nM), the fast inward pulse current is abolished, leaving a current that activates relatively slowly and does not inactivate significantly during the 7-ms pulse (Fig. 3*B*).

On return to −70 mV, the two phases of decay of the tail current seen in Fig.

2 are present both with and without TTX (Fig. 3, *A* and *B*). Na channels can, when not inactivated, produce rapid tail currents (cf. Fig. 5), but the fast, TTX-insensitive component in Fig. 3 must have a different origin. Further evidence identifying the currents in Fig. 3*B* as Ca current will be presented below.

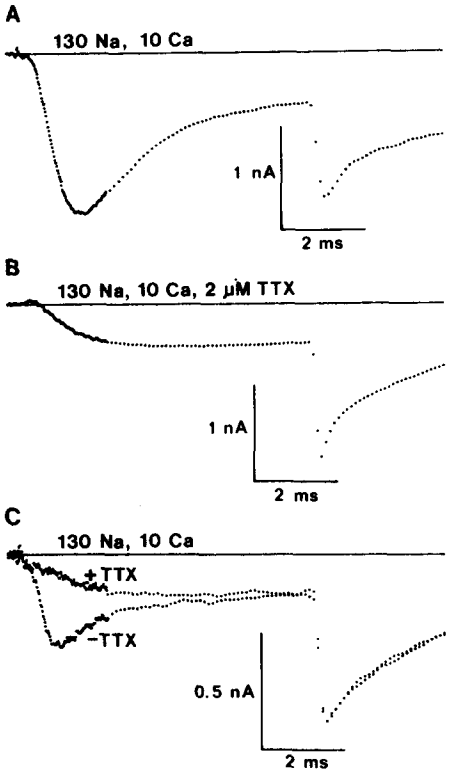

FIGURE 3. TTX blocks a fast inward current. Currents were generated at +20 mV, without (*A*) and with (*B*) 2 μM external TTX, which blocked the fast inward pulse current. The currents shown in *C* were recorded in a single cell before and after addition of TTX. They illustrate that virtually all of the current at the end of the 7-ms pulse and all of the tail current after it are insensitive to TTX. 130 Na, 10 Ca//130 Cs, 20 EGTA. Holding potential: (*A*) −70 mV, (*B* and *C*) −80 mV. Preparations: (*A*) JA203R, (*B*) MR303S, (*C*) AP113S.

In some cases it was possible to record currents from a single cell before and after adding TTX to the bath, as in Fig. 3*C*. TTX addition removes the fast inward pulse current and has almost no effect on the steady state current or the tail current.

Variability of Inward Current

The pattern of inward current illustrated in Fig. 2 was very common, but there was some variability from cell to cell. A few cells, for example, had little or no fast inward pulse current and/or the tails were relatively small in amplitude. The

explanation for this variability is not clear. A possible origin, suggested to us by C. Deutsch, is that the cells are not synchronized with respect to their growth phase, or the cells of the GH3 line may not be genetically uniform.

Reversal of the Fast Pulse Current

The fast inward pulse current reverses direction near the potential expected for a sodium-selective channel, as shown in Fig. 4. Fig. 4*A* was recorded in 140 Na,

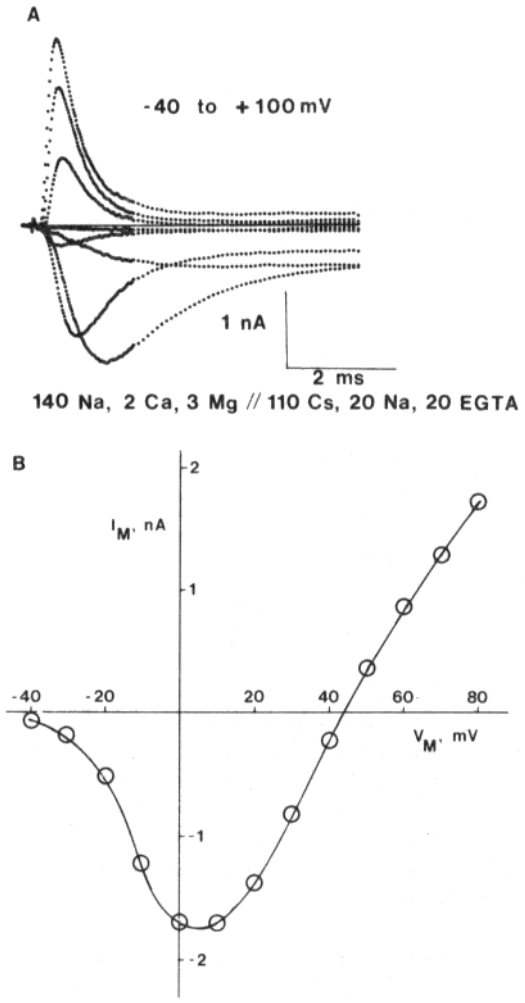

FIGURE 4. Reversal of the fast pulse current follows V_{Na}. The currents in *A* were generated by steps to −40 through +100 mV in 20-mV increments. The fast pulse current reverses direction, from inward to outward, between +40 and +60 mV. In *B*, the magnitude of the fast current is plotted as a function of membrane potential. Threshold for this component was about −40 mV and it reversed at about +45 mV. Solutions were 140 Na, 2 Ca, 3 Mg//110 Cs, 20 Na, 20 EGTA. Holding potential: −70 mV. Preparation JA213R.

2 Ca, 3 Mg//110 Cs, 20 Na, 20 EGTA, using steps from −40 to +100 mV in 20-mV increments. The current reverses direction between +40 and +60 mV. The magnitude of the fast pulse current is plotted as a function of voltage in Fig. 4*B*. Peak inward current magnitude increases steeply with voltage above a threshold of about −40 mV, reaches a maximum value between 0 and +10 mV, and reverses at about +45 mV. The Na equilibrium potential predicted from the Nernst equation with 140 mM Na^+ outside and 20 mM Na^+ inside is +49 mV, which is close to the observed reversal potential.

Thus, the fast pulse current reverses at or near the Na equilibrium potential and is blocked by TTX. There seems little doubt that this current is carried through Na channels.

Equilibration of Pipette Fluid with the Cell Interior

Fenwick et al. (1982*a*) reported that patch pipette solutions equilibrate rapidly and completely with the cell cytoplasm when used in the whole-cell recording configuration. This is also the case in our experiments as confirmed above. For example, when the pipette contained 140 mM Cs^+ and no K^+, the K currents were abolished within seconds (Fig. 2). Furthermore, when the pipette solution contained 20 mM Na^+, as in Fig. 4, the reversal of the Na current occurred near the potential expected for this concentration of internal Na^+. Thus, the ionic composition of the cell interior can be controlled by filling pipettes with the desired solution.

Inward Current in the Presence and Absence of Ca^{++}

The slow current during a pulse and the slow tail current after are small or absent when there is no external Ca^{++}, as illustrated in Fig. 5*A*. The continuous trace with superimposed dots is the Na current during a 7-ms pulse, which activates to a peak in <1 ms and spontaneously inactivates. The current at the end of the pulse is very small and must be carried through a small fraction of the Na channels that have not inactivated.

The current tails in the figure were generated by cutting short the pulse and returning to the holding potential after various intervals. Only a fast component of current is visible: the slow component is totally absent when there is no external Ca^{++}. The magnitude of each tail current increases for a short time after the step before decaying, probably because of the limited frequency response imposed by the series resistance. As expected, the envelope of the tails has the same time course as the current during the pulse.

Currents recorded with the same procedure are quite different in the presence of 10 Ca^{++} (Fig. 5*B*). There is substantial inward current remaining at the end of a maintained pulse (dots on a continuous line), and both activation and inactivation of the early current appear slower than in Fig. 5*A*. Some of the apparent slowing of inactivation probably results from overlap between slowly activating Ca current and inactivating Na current. After the shortest step (0.5 ms), the tail current has only a fast phase of decay. A small slow component is visible after a 1-ms step, and it grows rapidly as the step is lengthened. Concurrently, there is a decrease of the fast tail component. The 7-ms tail has a small fast component and a large slow one.

These current components can be reasonably identified as follows. The fast pulse current is carried through Na channels and is TTX sensitive (Fig. 3). Most of the maintained pulse current is through Ca channels, with a small contribution from Na channels that are not inactivated (Fig. 5). The rapidly deactivating tail current seen with short steps is carried through Na channels. It is present only when there is external Na, and it is TTX sensitive. The slow component of tail current is seen only when there is external Ca and is therefore carried by Ca ions through slowly deactivating Ca channels. The fast component of the tail current after a long step is probably a mixture of current through Na channels that have not inactivated (Fig. 5 *A*) and current through Ca channels, which have a fast component of deactivation (Fig. 3 *B*).

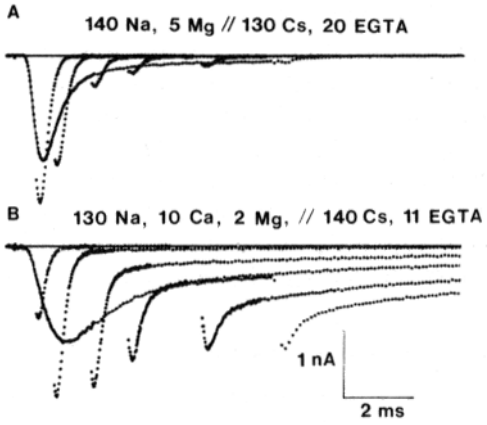

FIGURE 5. Ca dependence of inward currents. (*A*) The continuous trace is Na current at +20 mV, recorded in the absence of external Ca^{++}. The tail currents, recorded at −70 mV after pulses of various durations, have only a fast component of decay. The sustained pulse current and the tail at the end of a 7-ms pulse are almost absent in the absence of Ca^{++} (140 Na, 5 Mg//130 Cs, 20 EGTA). Holding potential: −70 mV. Preparation JA083R. (*B*) Currents generated by the same protocol as in *A*, but in the presence of 10 mM Ca, have a large sustained inward current at the end of the pulse. In addition, tails that follow steps of 1 ms or longer duration have two components of decay (130 Na, 10 Ca//140 Cs, 11 EGTA). Holding potential: −70 mV. Preparation JA203R.

Activation Voltage Range for Ca and Na Channels

Sodium and calcium channels in GH3 cells activate over somewhat different voltage ranges. Normalized conductances for the two ions are plotted as functions of membrane potential in Fig. 6. Sodium current-voltage relationships (Fig. 4 *B*) were used to calculate g_{Na}, using the equation

$$g_{Na} = I_{Na}/(V - V_{Na}).$$

Calcium tail currents following 7-ms steps to various potentials, which are proportional to the conductance activated during the pulse, were used as a

normalized measure of g_{Ca}. Data from four cells are averaged for the g_{Na} curve and from three cells for the g_{Ca} curve. The g_{Ca} data in 2 mM Ca^{++} were almost indistinguishable from those in 5 mM Ca^{++}, so these data were combined. From the averaged curves, sodium conductance has a threshold of about −40 mV, whereas ~10% of g_{Ca} has activated by this voltage. Conductance is half-maximal at about −18 mV for g_{Ca} and −10 mV for g_{Na}.

Na Channel Inactivation in the Steady State

Inactivation of Na current was evident in Fig. 5*A*, where the amplitude of the pulse and tail currents decayed with increasing pulse duration. As in nerve fibers

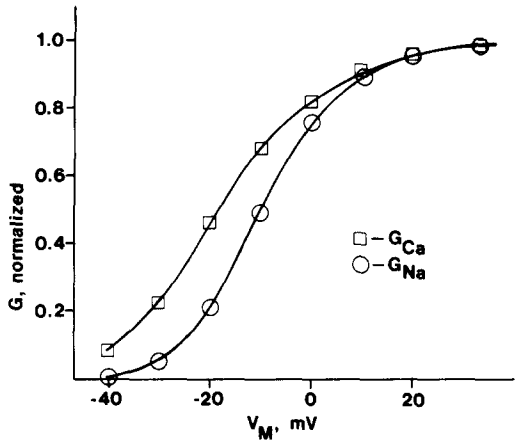

FIGURE 6. Activation voltage range for Na and Ca channels. Sodium conductance was calculated as described in the text, and the values were averaged over four cells and plotted as circles. I_{Na} was recorded in 140 Na, 5 Mg//130 Cs, 20 EGTA in one cell (JA083R), and in 140 Na, 2 Ca, 3 Mg//110 Cs, 20 Na, 20 EGTA in the others (JA213R). Calcium conductance values were averaged from three cells and plotted as squares. Since the $g_{Ca} - V$ curve in 2 mM Ca^{++} was almost indistinguishable from that in 5 mM Ca^{++}, we combined data from these two solutions. I_{Ca} was recorded in 140 Na, 2 Ca, 2 μM TTX//130 Cs, 20 EGTA in one cell (MR213S) and in 140 Na, 5 Ca, 2 μM TTX in the others (MR283R and AP113S). Curves were drawn by eye.

(Hodgkin and Huxley, 1952), the steady state level of Na channel inactivation is voltage dependent. This is illustrated in Fig. 7*A*, where the noninactivated fraction of the sodium current is plotted as a function of membrane potential. To generate this curve, we measured the Na current at +20 mV after 50-ms prepulses to the potential on the abscissa and plotted the current magnitude (relative to its maximum value) as a function of prepulse voltage. The data shown are average values from three cells. The midpoint of the curve is near −55 mV, and the noninactivated fraction of the current falls to <0.1 at −35 mV.

Recovery from Na Inactivation

After repolarization, Na channels in GH3 cells recover from inactivation over a

time course of several milliseconds, and the rate of recovery is voltage dependent. In the experiment of Fig. 7*B*, I_{Na} was inactivated by a 10-ms depolarization to 0 mV and then allowed to recover by repolarizing to a potential between −70 and −110 mV. Recovery was assessed by measuring I_{Na} during a test depolarization to 0 mV at various times following the prepulse. Fig. 7*B* shows semilog plots of the inactivated fraction of the Na current as a function of recovery time at −70 (×), −90 (filled circles), and −110 mV (open circles). Recovery rate is approxi-

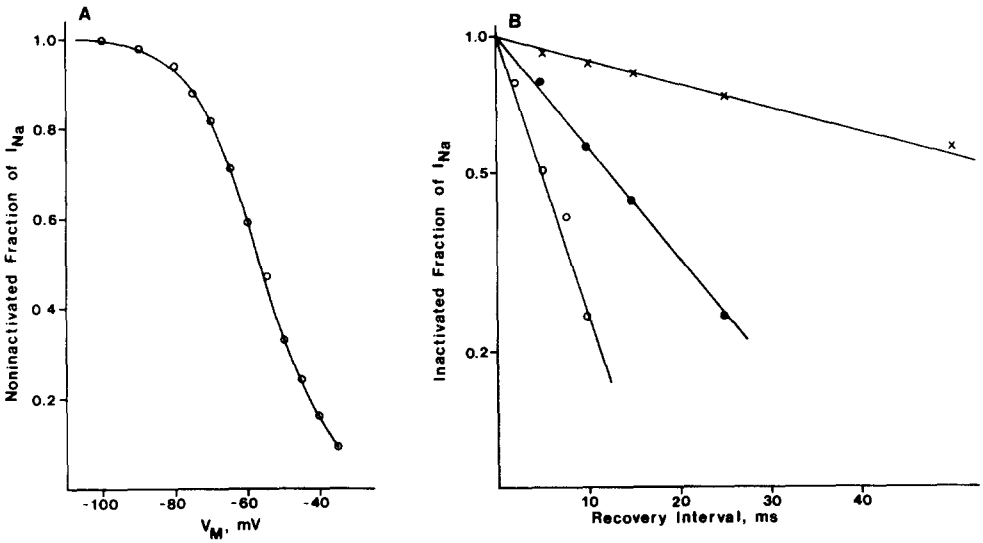

FIGURE 7. (*A*) Voltage dependence of steady state I_{Na} inactivation. I_{Na} during a test pulse to +20 mV was measured following 50-ms prepulses to various potentials, and normalized relative to its value at −100 mV. The normalized current, which is an estimate of the noninactivated fraction of I_{Na}, was averaged from three cells and plotted vs. prepulse voltage in the figure. The curve was drawn by eye. 140 Na, 2 Ca, 3 Mg//130 Cs, 20 EGTA. Holding potential: −80 mV. Preparation MR153R. (*B*) Recovery from I_{Na} inactivation was measured at three voltages in a single cell. Na channels were inactivated by a 10-ms depolarization to 0 mV and then allowed to recover at −70 (×), −90 (filled circles), or −110 mV (open circles). The noninactivated fraction of I_{Na} was determined by measuring the current in response to a test pulse to 0 mV at various times after repolarization and normalizing relative to I_{Na} in the absence of a prepulse. The lines are linear least-squares fits to the log transformed data, which gave the following estimates of the recovery time constant: 119 ms at −70, 17.4 ms at −90, and 7.0 ms at −110 mV. Holding potential: −80 mV. Preparation MR153S. Same solutions as in *A*.

mately exponential, and the time constants (determined from least-squares fits) from this cell and two others are given in Table II.

Inactivation of Ca Channels

For depolarizations longer than 10 ms, Ca current decays significantly during the pulse, which suggests that the channels are inactivating. The current in Fig. 8*A* was generated by a 100-ms voltage-clamp step to +10 mV, in 130 Na, 10 Ca,

TTX//130 Cs, 20 EGTA. The current activates to a peak in ~10 ms and then declines to 25% of its peak value at the end of the pulse.

The waveform in Fig. 8*A* could be the result of an activating outward current carried by residual K ions in the cell, or an inactivating inward current. To distinguish between these two possibilities, we measured the tail currents at the end of the pulse, and from them ascertained whether membrane conductance was increasing or decreasing. The tail currents are illustrated in Fig. 8*B*, and were recorded in the absence of Na ion (35 mM Ca//150 Cs) after depolarizations to +20 mV for the indicated durations. The first few data points in each trace are a current baseline, taken before the activating pulse. Sampling was then stopped and resumed at the end of the activating pulse. The records thus show baseline current in the final 400 μs of the activating pulse, and the current during and after a step back to the holding potential. The records illustrate that the instantaneous change in current upon repolarization decreases as the activating pulse is made longer. Membrane conductance is thus decreasing during the pulse, which proves that the Ca channels are inactivating.

Ca Inactivation and Ca Accumulation

It has been shown in molluscan neurons (Tillotson, 1979) and in paramecium

TABLE II

Time Constants (in Milliseconds) of Recovery from I_{Na} Inactivation

	V_M		
Cell	−70 mV	−90 mV	−110 mV
1	31	9.2	4.3
2	118	17.4	7.0
3	63	14.4	5.4

(Brehm and Eckert, 1978) that inactivation of Ca channels results from accumulation of Ca^{++} inside the cell. We have tested this hypothesis in GH3 cells by measuring inactivation with the tail procedure in the presence of high concentrations of internal EGTA. Fig. 8*C* shows an example with 50 mM EGTA in the pipette and should be compared with Fig. 8*B*, where no EGTA was present. The rate and extent of inactivation are not significantly affected by the presence of EGTA. Estimates of the time constant of inactivation from several cells in the presence or absence of EGTA are shown in Table III. The inactivation rate in 50 mM EGTA is not significantly different from the rate in the absence of EGTA. There seems little doubt that EGTA enters the cell in high concentration, because of the results on equilibration presented above. It is thus hard to escape the conclusion that in GH3 cells, inactivation of Ca channels does not result from Ca accumulation in any space accessible to EGTA in the cell interior. The inactivation mechanism here thus seems to be different from the convincingly demonstrated mechanism in molluscan neurons.

Ca Inactivation and Membrane Potential

The degree of Ca channel inactivation as a function of membrane potential was measured with the two-pulse procedure that is diagrammed in the inset of Fig.

9. A prepulse of 100 ms duration was applied, taking V_m to the potential plotted on the abscissa. A test pulse to +10 mV for 7 ms then fully activated the Ca channels still capable of conducting, and Ca conductance was determined from the tail current that followed this activating pulse. Steady state inactivation is a

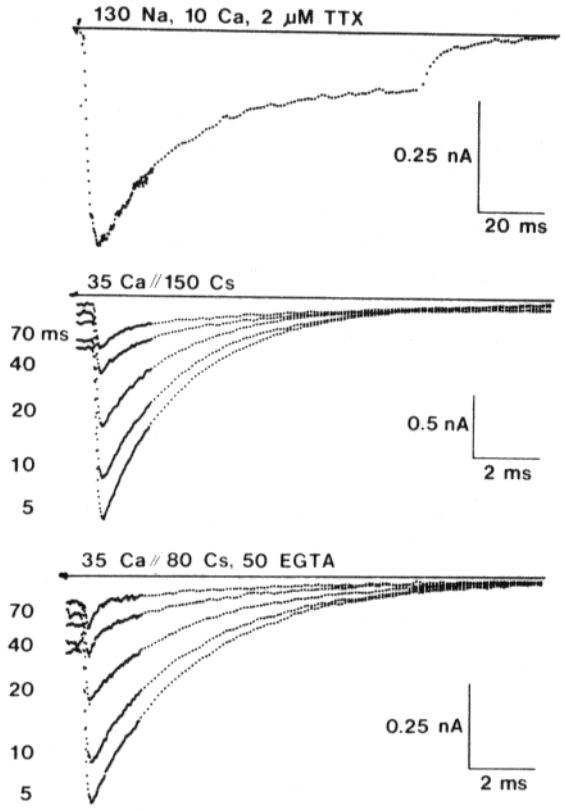

FIGURE 8. Calcium channel inactivation. The calcium current in *A* was recorded at +10 mV. The current decay during the pulse suggests that the channels are inactivating. The tail currents in *B* and *C* were recorded after depolarizations to +20 mV for the indicated durations. The first few data points were taken before the pulse to provide a current baseline. Sampling was then stopped and restarted shortly before the activating pulse ended. *B* and *C* illustrate that conductance decreases as a function of pulse duration, which demonstrates that the Ca channels inactivate. Solutions: (*A*) 130 Na, 10 Ca, 2 μM TTX//130 Cs, 20 EGTA; (*B*) 35 Ca//150 Cs; (*C*) 35 Ca//80 Cs, 50 EGTA. Holding potential: −80 mV. Preparations: (*A*) MR303S, (*B*) AU293R, (*C*) AU223S.

steep, S-shaped function of V_m, with a midpoint about −47 mV. This voltage is near the foot of the calcium activation curve plotted in Fig. 6.

Experiments of two other types show that, as in other cells, inactivation becomes less complete as voltage is made more positive. Currents during long pulses are shown in Fig. 10. It is clear from the traces that inactivation is relatively

TABLE III

Time Constants (in Milliseconds) of I_{Ca} Inactivation

	Solution		
Observation	150 Cs	130 Cs, 20 EGTA	80 Cs, 50 EGTA
1	26.9	21.1	33.3
2	30.9	28.2	31.0
3	14.3	25.0	20.1
4	25.3	30.2	23.2
5	18.6	22.4	29.9
6	21.8	—	19.2
Mean ± SD	23±6	25±4	26±6

complete at −30 mV, and that at higher voltage it is faster but progressively less complete.

The same conclusion is reached when inactivation is assayed from tail currents, following activating pulses of different amplitudes, as illustrated in Fig. 11. The baselines for the traces in the figure are drawn through points taken before the activating pulse. Sampling was then stopped and resumed just before the activating pulse ended. Fig. 11 *A* shows tails for pulses lasting 10 and 100 ms to 0 mV; in Fig. 11 *B* the voltage was +60 mV, again for 10 and 100 ms. At both voltages

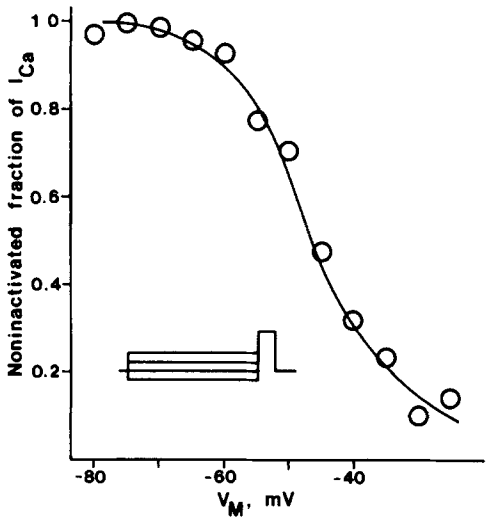

FIGURE 9. Voltage dependence of I_{Ca} inactivation. The inset illustrates the pulse protocol used to measure Ca channel inactivation. A 7-ms test depolarization to +10 mV followed 100-ms prepulses to the voltages indicated on the abscissa. The noninactivated fraction of the Ca channels was determined by measuring the Ca^{++} tail current at −80 mV following the test step. The magnitude of the tail, normalized relative to its maximum value, was averaged from two cells and plotted as a function of prepulse voltage. 140 Na, 5 Ca, 2 μM TTX//130 Cs, 20 EGTA. Holding potential: −80 mV. Preparation MR283R.

the tails have a fast component of decay and a slow one. The fast component is more prominent at +60 mV, and is particularly striking after the 100-ms pulse at this voltage. The slow component is large after the 10-ms pulse and much reduced after 100 ms. Inactivation was assayed by measuring peak tail current magnitude (without extrapolation). At 0 mV, current after 100 ms was 28% of that after 10 ms; at +60 mV, it was 68%. Inactivation thus is substantially less complete at +60 mV than at 0 mV. Fig. 11, *C* and *D*, shows similar behavior from another cell. In both cases it seems that the noninactivated component of the current after the long pulse decays very rapidly after repolarization.

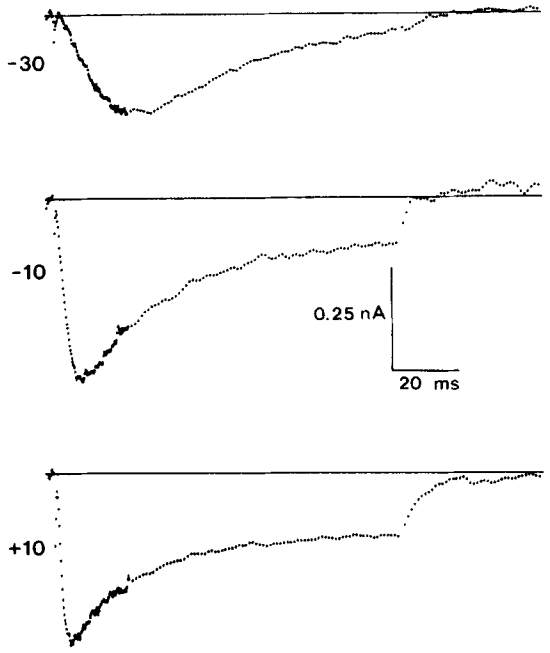

FIGURE 10. I_{Ca} inactivation decreases at positive voltages. Currents were generated by 100-ms steps to the indicated voltages. Inactivation occurs faster at more positive potentials, but is less complete. 130 Na, 10 Ca, 2 μM TTX//130 Cs, 20 EGTA. Holding potential: −80 mV. Preparation MR303S.

Behavior of Ca Channels with Ba^{++} as Charge Carrier

Calcium channels in GH3 cells show some alterations in behavior when Ba^{++} replaces Ca^{++} as the charge carrier. Barium ions carry current more effectively than Ca^{++}, and the current does not inactivate appreciably. A typical Ba^{++} current is shown in Fig. 12*A*. The current declines very little after reaching its peak value, which indicates that the channels are not inactivating. This is confirmed by comparing Ba^{++} tail currents following a 10-ms and a 100-ms depolarization to +20 mV (Fig. 12*B*). The sampling protocol for these records was the same as in Fig. 8, *B* and *C*. Although the time course is quite different,

the initial tail amplitude is the same for the two traces, and, by this index, there is no inactivation.

After the 10-ms step, the Ba^{++} current deactivates with a fast and a slow phase, the pattern usually seen with Ca^{++} currents (cf. Figs. 3*B* and 11). The fast phase is more prominent with Ba^{++} and accounts for a larger fraction of total tail current. Interestingly, the slow component of deactivation is almost gone after the 100-ms activating pulse in Fig. 12*B*. The slow tail component in Ba^{++} diminishes with approximately the same time course that Ca^{++} current inactivates (Figs. 8 and 11). This suggests that the process which results in inactivation of

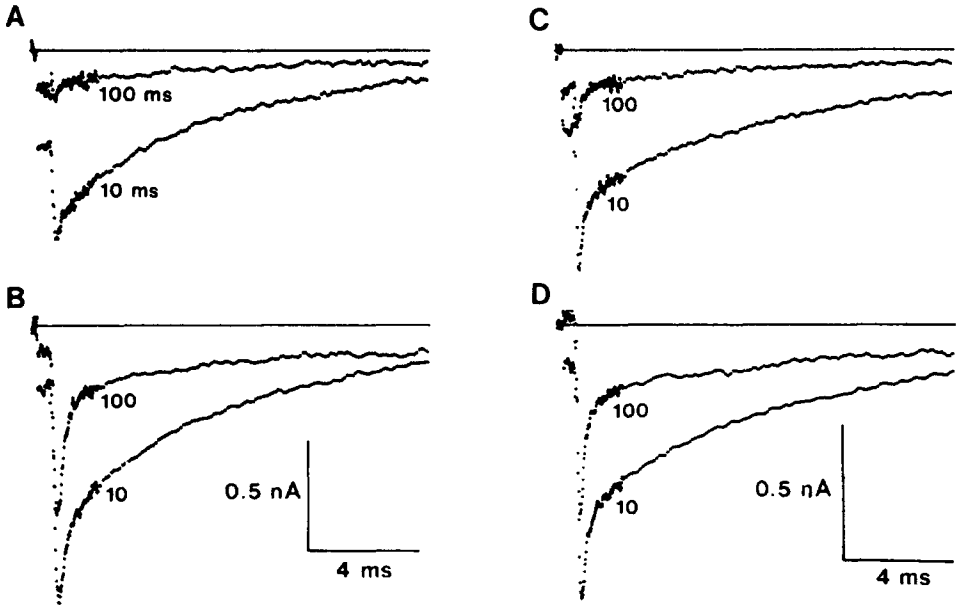

FIGURE 11. Inactivation of Ca^{++} tail currents is less complete at positive potentials. Each panel illustrates tail currents following both 10- and 100-ms depolarizations to 0 (*A*) and +60 mV (*B*) in one cell and to +10 (*C*) and +60 mV (*D*) in another. The decline in tail magnitude with increasing pulse duration is much more pronounced at 0 or +10 mV than at +60 mV. 130 Na, 10 Ca//130 Cs, 20 EGTA. 2 μM TTX was present in *C* and *D*. Holding potential: −70 mV. Preparation JA253R.

the Ca^{++} current is still present with Ba^{++} as the current carrier, but in the latter case it results in fast deactivation of the current rather than inactivation. In general, the behavior is similar to the Ca currents at +60 mV in Fig. 11, but the fast component is more prominent and is seen at a lower voltage.

Inactivation can be restored by adding a few millimolar Ca^{++} to the Ba^{++} medium. The tail currents in Fig. 12*C* were recorded in 35 Ba, 5 Ca//130 Cs, 20 EGTA. They resemble the ones in Fig. 8, *B* and *C*, recorded in 35 Ca, and clearly show that inactivation has occurred during the pulse. Thus, Ca^{++} in the external fluid is required for inactivation and Ba^{++} cannot substitute.

Na Channels Recover More Rapidly than Ca Channels

The kinetics of recovery from inactivation reported above imply that Ca channels should remain inactivated long after Na channels have recovered. This was tested in the experiment of Fig. 13. The two traces were recorded at +40 mV in 140 Na, 10 Ca//140 Na. Under these conditions I_{Na} is outward. The dotted trace is the control and shows a rapidly activating and inactivating outward Na current

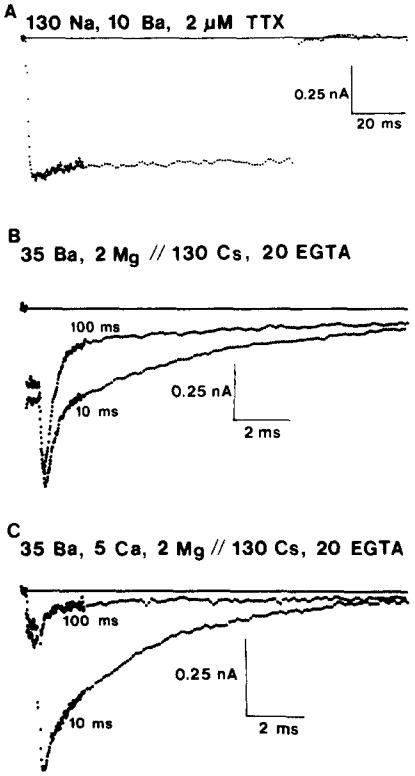

FIGURE 12. Ca channels do not inactivate in Ba^{++}. The Ba^{++} current in *A* was recorded at +10 mV and shows very little inactivation. The tail currents in *B* and *C* were recorded after depolarizations to +20 mV for the indicated durations. In the absence of Ca^{++} (*B*), tail magnitude does not decrease as a function of pulse duration. Inactivation could be restored by adding 5 mM Ca^{++} in the presence of Ba^{++} (*C*). Solutions were: (*A*) 130 Na, 10 Ba, 2 μM TTX//130 Cs, 20 EGTA; (*B*) 35 Ba//130 Cs, 20 EGTA; (*C*) 35 Ba, 5 Ca//130 Cs, 20 EGTA. Holding potential: (*A*) −80 mV, (*B* and *C*) −70 mV. Preparations: (*A*) MA023S, (*B*) JA183R, (*C*) JA053R.

during the depolarization and a Ca tail current following repolarization. The solid trace was recorded 100 ms after an inactivating prepulse of 100 ms duration to +20 mV. The Na current has almost completely recovered from inactivation, while the Ca current, as judged from the tail, is still largely inactivated. This result implies that under appropriate circumstances GH3 cells could generate Na action potentials without much Ca entry.

DISCUSSION

Whole-Cell Recording with the Patch-Clamp Technique

The whole-cell currents shown in this paper demonstrate that voltage-clamp records of good quality can be obtained with the gigaseal technique (cf. Fenwick et al., 1982*b*). The signal-to-noise ratio of these currents is almost as good as can be obtained with a squid axon voltage clamp, although time resolution is as yet inferior. The time required to impose a voltage-clamp step can be reduced by using electrodes of very low resistance, by ballistically charging the membrane (as described in Methods), and by using series resistance compensation. Overall, the response time is good enough for measuring tail currents with reasonable fidelity, even at room temperature. The ability to record currents under accurate space and voltage-clamp conditions will obviously be useful in studying membrane

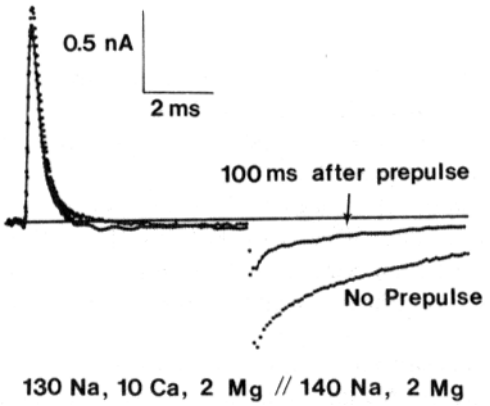

FIGURE 13. Recovery of I_{Na} and I_{Ca} from inactivation. Currents were recorded at +40 mV either in the absence of a prepulse (dotted trace) or 100 ms after a 100-ms step to +20 mV (line with superimposed dots). After the prepulse, I_{Na} was almost completely recovered from inactivation, whereas I_{Ca} was still largely inactivated. 130 Na, 10 Ca//140 Na. Holding potential: −70 mV. Preparation FE073R.

conductances in a wide variety of cell types. The technique has already been applied to chromaffin cells (Fenwick et al., 1982*a*, *b*), human lymphocytes (Matteson and Deutsch, 1984), and of course anterior pituitary cells (see also Hagiwara and Ohmori, 1982, and Dubinsky and Oxford, 1982).

Currents in GH3 Cells

Much of the previous evidence concerning ionic channels in GH3 cells has come from studies of the effect of ionic substitution or channel blockers on the action potential. It has been reported that the spike is blocked by either Mn^{++} (Kidokoro, 1975) or D600 (Taraskevich and Douglas, 1980), but not by TTX, which suggests that Ca channels are responsible for spiking. In another study, both Na and Ca channels were implicated, because electrical activity persisted in either TTX or Mn^{++}, but not in the presence of both (Biales et al., 1977). The apparent lack of a sodium component in some reports could have been due to low resting

potentials (−40 mV in Kidokoro, 1975), which would have left Na channels largely inactivated (cf. Fig. 7*A*). In agreement with this idea are the results of Ozawa and Miyazaki (1979), who found that a Ca^{++}-free media plus 2–4 mM Co^{++}, action potentials could be elicited with depolarizing current pulses only if the cell was hyperpolarized to −55 to −65 mV. Na and Ca channel activity in GH3 cells has been observed directly by Hagiwara and Ohmori (1982; cf. Dubinsky and Oxford, 1982) using the gigaseal technique.

Pituitary cells are reported in many cases to be spontaneously active. In pars intermedia cells, the Ca channel blockers Co^{++}, Ni^{++}, or Mn^{++} decreased spontaneous action potential frequency (Douglas and Taraskevich, 1982). This suggests that Ca channels may generate pacemaker current, but the precise ionic basis for pacemaking remains to be determined. Fig. 6 in this paper suggests that Ca channels are more likely to be involved than Na channels, for they activate in a more negative voltage range.

Na Channels

Our results, and those of others, clearly show the presence of Na channels in GH3 cells, although at rather low density. The maximum current density that we have measured, calculated on the basis of a spherical cell with no infolding, is ~0.2 mA/cm^2, which is more than 10 times smaller than the current density in squid axon membrane. The channels have properties similar to Na channels in squid nerve, but there are differences. For one thing, their activation range is somewhat more positive than Na channels in nerve fibers. Further, inactivation in GH3 cells is quite fast relative to activation, particularly at positive voltages (Fig. 4*A*).

The last-mentioned result has an interesting implication for the mechanism of inactivation. We fitted the Na currents from GH3 cells with two simple models of inactivation: the Hodgkin and Huxley (1952) model, in which inactivation is independent of activation, and a model in which the two gating processes are strictly coupled, which means that Na channels must activate fully before inactivating. (Observations from nerve show that full activation is not required, but this matters little to the calculations presented here.) Theoretical Na currents based on either of these models accurately fit the data, as shown in Fig. 14. The models give quite different predictions, however, of the fraction of Na channels open at the peak of the current: 24% for the H-H model and 54% for the coupled model. We have no data from GH3 cells to choose one model over the other, but a coupled model of the type applicable to nerve (Bezanilla and Armstrong, 1977; Armstrong and Bezanilla, 1977) clearly would result in more efficient use of the Na channels and thus make possible a lower density.

Ca Channels

It is clear from the literature that agreement has not been reached on the degree and mechanism of inactivation of Ca channels (e.g., Hagiwara and Byerly, 1981; Reuter, 1983; Tsien, 1983). Either there are several types of Ca channels, or there are significant differences in the methods and conditions of recording. Regarding inactivation, our conclusions about GH3 cells differ from the other-

wise excellent results of Hagiwara and Ohmori (1982), who argued that the decline in Ca current during depolarization in GH3 cells arises not from inactivation, but from the activation of an outward current. We completely eliminated outward current by filling the cells with Cs^+, and we still saw inactivation. Further, the behavior of the Ca tail currents (Fig. 8) shows clearly that step conductance decreases as a function of pulse duration and provides clear evidence that Ca channels inactivate when external Ca^{++} is present.

After replacement of all external Ca^{++} by Ba^{++}, Ca channels inactivate much less, if at all. At first glance, the failure to inactivate in Ba^{++} seems to fit well with the proposal that Ca^{++} accumulation in the cell interior is responsible for inactivation. This has been demonstrated quite convincingly in molluscan cells, where injection of EGTA slows inactivation of the Ca current (Tillotson, 1979).

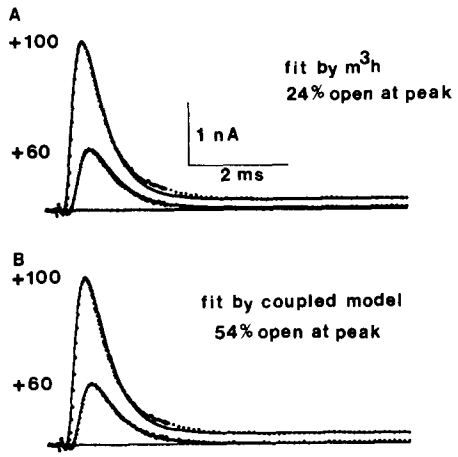

FIGURE 14. I_{Na} calculations based on two models of inactivation. The Na currents recorded at +60 and +100 mV (dotted traces) were taken from the experiment illustrated in Fig. 4. The smooth curves were calculated either from the Hodgkin and Huxley model in *A*, or a sequential model in which the channels must open before they inactivate (*B*).

The same experiment performed in GH3 cells provides a different result: inactivation rate is unchanged for EGTA concentrations in the pipette as high as 50 mM. We are forced to conclude that inactivation of Ca channels in GH3 cells does not result from Ca accumulation.

Replacement of Ca^{++} by Ba^{++} shows quite clearly, however, that external Ca^{++} (or, possibly, an undiscovered substitute) is in some way required for inactivation of pulse current. Perhaps the most intriguing result in the paper is the behavior of the current tails in Ba^{++} with no Ca^{++} present. We are aware of no precedents for this behavior. The fast component of decay that is visible in Ca^{++}-containing solutions (Figs. 3 and 11) is accentuated, and the slow component is relatively smaller after a short-duration step. After a long step, the slow component is reduced or absent, and the fast component may be larger. The evolution of these changes occurs with about the same time course as inactivation in the presence

of Ca^{++}. Thus, there seems to be an underlying process following depolarization that progresses with or without external Ca^{++}. If Ca^{++} is present outside, the process results in inactivation; if only Ba^{++} is present, there is no inactivation during a long pulse, but there is rapid deactivation following it.

In 10 mM Ca^{++} at positive voltages there are manifestations of the same behavior seen in Ba^{++} (Figs. 11 and 12). Preliminary results suggest that this behavior is also prominent in 2 mM Ca^{++} and may have some physiological relevance. Further investigation may give some insight into the mechanism as well as the relevance to function.

We have not studied the activation kinetics of Ca channels with great care, and modeling along Hodgkin and Huxley lines seems premature until we have single-channel records as well as macroscopic currents. The complexity of deactivation kinetics and their dependence on pulse duration and ion composition make it clear that a simple model is unlikely to suffice.

Comparison with Ca and Na Channels in Other Tissues

Na and Ca channel properties may vary from tissue to tissue, and, consistent with this idea, some of the properties of channels in GH3 cells are significantly different from those in, for example, chromaffin and heart cells. One difference is in the activation range. Na channels in heart cells activate and inactivate to the left (negative) of Ca channels on the voltage axis (e.g., Reuter, 1983), while just the opposite holds in GH3 cells. This is true even in low external Ca^{++} concentrations, and thus cannot be attributed to a positive shift of Na channel activation range by Ca^{++}. Comparison with data from heart suggests that on an absolute scale, GH3 Ca channels are left-shifted, and Na channels are right-shifted relative to Ca and Na channels in heart.

From the records of Lee and Tsien (1982), Ca channels in heart activate about as rapidly as in GH3 cells, requiring 2 or 3 ms to peak at about 21°C at +20 mV. With K^+ inside, heart Ca channels seem to activate more slowly than with Cs^+, requiring 40 ms at 37°C (voltage unspecified; Marban and Tsien, 1982). Lee and Tsien (1982) found that outward currents through heart Ca channels at +90 mV inactivate in the absence of permeant divalent cations. We have no data at +90 mV, but at lower voltages inactivation in GH3 cells seems to require external Ca^{++}, as described above.

Many questions remain to be examined using this excellent new preparation. Among them are the rate and voltage dependence of Ca channel inactivation, and more generally the mechanism; the Na^+ permeability of the Ca channels; the response to Ca channel blockers; the behavior of Ca channels at lower Ca^{++} concentration; the ionic basis of pacemaking; and the effects of secretagogues on ionic channels.

Received for publication 14 June 1983 and in revised form 6 September 1983.

REFERENCES

Adelman, W. J., Jr., and J. P. Senft. 1966. Voltage clamp studies of the effect of internal cesium ion on sodium and potassium currents in the squid giant axon. *J. Gen. Physiol.* 50:279–293.

Armstrong, C. M., and F. Bezanilla. 1974. Charge movement associated with the opening and closing of the activation gates of the Na channel. *J. Gen. Physiol.* 63:533–552.

Armstrong, C. M., and F. Bezanilla. 1977. Inactivation of the sodium channel. II. Gating current experiments. *J. Gen. Physiol.* 70:567–590.

Armstrong, C. M., and S. R. Taylor. 1980. Interaction of barium ions with potassium channels in squid giant axons. *Biophys. J.* 30: 473–488.

Bezanilla, F., and C. M. Armstrong. 1972. Negative conductance caused by entry of sodium and cesium ions into the potassium channels of squid axons. *J. Gen. Physiol.* 60:588–608.

Bezanilla, F., and C. M. Armstrong. 1977. Inactivation of the sodium channel. I. Sodium current experiments. *J. Gen. Physiol.* 70:549–566.

Biales, B., M. A. Dichter, and A. Tischler. 1977. Sodium and calcium action potential in pituitary cells. *Nature (Lond.).* 267:172–174.

Brehm, P., and R. Eckert. 1978. Calcium entry leads to inactivation of calcium channel in *Paramecium. Science (Wash. DC).* 202:1203–1206.

Douglas, W. W., and P. S. Taraskevich. 1982. Slowing effects of dopamine and calcium-channel blockers on frequency of sodium spikes in rat pars intermedia cells. *J. Physiol. (Lond.).* 326:201–211.

Dubinsky, J. M., and G. S. Oxford. 1982. Comparison of ionic currents in voltage-clamped pituitary tumor cells in culture. *Soc. Neurosci. Abstr.* 8:60.

Dufy, B., and J. L. Barker. 1982. Calcium-activated and voltage-dependent potassium conductances in clonal pituitary cells. *Life Sci.* 30:1933–1941.

Eaton, D. C., and M. S. Brodwick. 1980. Effects of barium on the potassium conductance of squid axon. *J. Gen. Physiol.* 75:727–750.

Fenwick, E. M., A. Marty, and E. Neher. 1982*a*. A patch-clamp study of bovine chromaffin cells and of their sensitivity to acetylcholine. *J. Physiol. (Lond.).* 331:577–597.

Fenwick, E. M., A. Marty, and E. Neher. 1982*b*. Sodium and calcium channels in bovine chromaffin cells. *J. Physiol. (Lond.).* 331:599–635.

Hagiwara, S., and L. Byerly. 1981. Calcium channel. *Annu. Rev. Neurosci.* 4:69–125.

Hagiwara, S., and H. Ohmori. 1982. Studies of calcium channels in rat clonal pituitary cells with patch electrode voltage clamp. *J. Physiol. (Lond.).* 331:231–252.

Hamill, O. P., A. Marty, E. Neher, B. Sakmann, and F. J. Sigworth. 1981. Improved patch-clamp techniques for high-resolution current recording from cells and cell-free membrane patches. *Pflügers Arch. Eur. J. Physiol.* 391:85–100.

Hodgkin, A. L., and A. F. Huxley. 1952. A quantitative description of membrane current and its application to conduction and excitation in nerve. *J. Physiol. (Lond.).* 117:500–544.

Kidokoro, Y. 1975. Spontaneous calcium action potentials in a clonal pituitary cell line and their relationship to prolactin secretion. *Nature (Lond.).* 258:741–742.

Lee, K. S., and R. W. Tsien. 1982. Reversal of current through calcium channels in dialyzed single heart cells. *Nature (Lond.).* 297:498–501.

Marban, E., and R. W. Tsien. 1982. Effects of nystatin-mediated intracellular ion substitution on membrane currents in calf Purkinje fibers. *J. Physiol. (Lond.).* 329:569–587.

Matteson, D. R., and C. Deutsch. 1984. K channels in T lymphocytes: a patch clamp study using monoclonal antibody adhesion. *Nature (Lond.).* In press.

Matteson, D. R., and C. M. Armstrong. 1983. Voltage clamp experiments on GH3 cells. *Biophys. J.* 41:223*a*. (Abstr.)

Ozawa, S., and S. Miyazaki. 1979. Electrical excitability in the rat clonal pituitary cell and its relation to hormone secretion. *Jpn. J. Physiol.* 29:411–426.

Reuter, H. 1983. Calcium channel modulation by neurotransmitters, enzymes, and drugs. *Nature (Lond.)*. 301:569–574.

Taraskevich, P. S., and W. W. Douglas. 1977. Action potentials occur in cells of the normal anterior pituitary gland and are stimulated by the hypophysiotropic peptide thyrotropin-releasing hormone. *Proc. Natl. Acad. Sci. USA*. 74:4064–4067.

Taraskevich, P. S., and W. W. Douglas. 1980. Electrical behavior in a line of anterior pituitary cells (GH cells) and the influence of the hypothalamic peptide, thyrotropin releasing factor. *Neuroscience*. 5:421–431.

Tillotson, D. 1979. Inactivation of Ca conductance dependent on entry on Ca ions in molluscan neurons. *Proc. Natl. Acad. Sci. USA*. 76:1497–1500.

Tsien, R. W. 1983. Calcium channels in excitable cell membranes. *Annu. Rev. Physiol.* 45:341–358.